Borromean states in a one-dimensional three-body system

Tobias Schnurrenberger [1], Lucas Happ [2], and Maxim A. Efremov [1,*]
[1] German Aerospace Center (DLR), Institute of Quantum Technologies, 89081 Ulm, Germany
[2] Few-body Systems in Physics Laboratory, RIKEN Nishina Center, Wakō 351-0198, Japan

(Received 27 May 2024; accepted 11 November 2024; published 23 January 2025)

We show the existence of Borromean bound states in a one-dimensional quantum three-body system composed of two identical bosons and a distinguishable particle. It is assumed that there is no interaction between the two bosons, while the mass-imbalanced two-body subsystems can be tuned to be either bound or unbound. Within the framework of the Faddeev equations, the three-body spectrum and the corresponding wave functions are computed numerically. In addition, we identify the parameter-space region for the two-body interaction, where the Borromean states occur, evaluate their geometric properties, and investigate their dependence on the mass ratio.

DOI: 10.1103/PhysRevResearch.7.013090

I. INTRODUCTION

Few-body physics plays a central role in the fields of ultracold quantum gases [1], nuclear physics [2], and hadron physics [3]. Special attention is given to three-body systems that have resonantly interacting two-body subsystems because they often show universal properties that are independent of the details of their short-range potentials [4]. Three-body bound states can even exist in situations when all of the two-body subsystems are unbound; those states are then named *Borromean* states [5,6].

In three spatial dimensions, a two-body system with an overall attractive potential may be unbound, when the interaction is weak enough. A system of three identical bosons with the same pairwise interaction can, however, be bound. Therefore there is a window for the coupling constant where Borromean states can occur [7]. The Efimov effect is a well-known example displaying such a behavior [8,9], and the theoretical predictions have been verified successfully in many experiments [6]. Moreover, such Borromean binding plays an essential role in subatomic physics, e.g., in halo nuclei [5,10,11]. In addition, those nuclei in three dimensions have been modeled by one-dimensional three-body systems [12].

When the particles are restricted to a two-dimensional plane, the situation is different. Here a two-body interaction with an overall attractive contribution always supports a bound state [13]. Therefore the bound states of a three-body system with such two-body interactions are not Borromean. Nevertheless, it has been shown that Borromean three-body states can exist in two dimensions by adding a repulsive contribution to the two-body interaction potential [14,15].

It is challenging to find or observe Borromean states in a one-dimensional setup, as the underlying two-body systems, similar to two dimensions, almost always have a bound state for an overall attractive potential [13]. However, for the special case of a continuously scale-invariant two-body potential, which does not fulfill all conditions considered in Ref. [13], the coupling can be tuned so that the two-body subsystem supports an infinite amount of bound states or none at all. For the latter case, it has been shown that an infinite number of Borromean states exists in the corresponding three-body system [16].

In this article we consider a one-dimensional three-body system consisting of two types of particles with different masses. They interact via a potential that has separate attractive and repulsive contributions. In this way, the parameters for this potential can be chosen such that the two-body system can be tuned continuously between two regimes to support either one or zero bound states. Such a smooth tuning allows us to identify the origin of the Borromean states. We solve the three-body system numerically with the Faddeev equations in momentum space [17] and find that this three-body system indeed has Borromean states. Moreover, we identify their region of existence in the parameter space of the two-body interaction and analyze their geometric properties. In addition, we find that the number of Borromean states increases for larger mass ratios.

Considering the experimental feasibility, quasi-one-dimensional systems in the form of cigar-shaped traps have been realized [18,19]. The interaction between different types of atoms can be adjusted with Feshbach resonances [20,21] or confinement-induced resonances [22,23]. To realize our system, cold dipoles which are aligned by an external field and confined to multiple quasi-one-dimensional tubes is a promising setup. The effective dipole-dipole interaction within the same or different tubes can be adjusted by the relative angle between the external field and the tube alignment [24,25]. Thus, the necessary ingredients to experimentally verify the theoretical predictions of this article are fully accessible with current experimental techniques.

*Contact author: maxim.efremov@dlr.de

The article is organized as follows. In Sec. II we introduce the underlying two-body subsystems as well as the corresponding three-body system. We also discuss the Faddeev equations that we use in our numerical calculations. Then, in Sec. III we show from our numerical results the existence of Borromean states and their dependence on the system parameters. In Sec. IV we propose an experimental setup to verify our theoretical predictions. In Sec. V we summarize our findings. The Appendixes A, B, and C provide further details on our calculations.

II. TWO- AND THREE-PARTICLE SYSTEMS

A. Two-particle subsystem

We start from a one-dimensional two-particle system consisting of distinguishable particles with masses M and m. The stationary Schrödinger equation for the two-particle wave function $\psi^{(2)}(x)$ is then given by

$$\left[-\frac{1}{2}\frac{\mathrm{d}^2}{\mathrm{d}x^2} + v(x)\right]\psi^{(2)}(x) = \mathcal{E}^{(2)}\psi^{(2)}(x), \tag{1}$$

with an interaction potential $v(x)$. A two-body potential in one dimension with $\int \mathrm{d}x\, v(x) < 0$ always has a bound state [13]. In contrast, a single repulsive barrier does not support a bound state. In order to be able to tune the system between a bound and unbound regime, we need both an attractive and repulsive term. For simplicity, and in order to treat the two-body system analytically, we consider a potential consisting of two δ distributions,

$$v(x) = -v_0\left[\delta\left(x - \tfrac{1}{2}\right) - \alpha\delta\left(x + \tfrac{1}{2}\right)\right], \tag{2}$$

with the parameters $v_0 > 0$ and α, describing the magnitudes of the overall potential and its relative repulsive contribution, respectively. An interaction potential adapted for a possible experimental setup employing dipoles is discussed later in Sec. IV.

Both equations (1) and (2) are presented in dimensionless variables. The position coordinate x is measured in units of the distance a between the two δ functions. The potential strength v_0 and the two-particle energy $\mathcal{E}^{(2)}$ are both given in units of a characteristic energy $\hbar^2/\mu a^2$, where $\mu = Mm/(M+m)$ is the reduced mass.

In Appendix A we solve Eq. (1) analytically, derive a transcendental equation for the two-particle energy $\mathcal{E}^{(2)}$, and discuss the number of solutions depending on α. For $v_0 > 0$ we can distinguish four regions in the parameter space (α, v_0), Fig. 1, with different numbers of bound and virtual states in our two-body subsystem. Virtual or antibound states correspond to poles of the two-body S matrix, which are on the negative imaginary axis of the complex momentum plane. These states have negative energies, and their wave functions grow exponentially and are therefore not normalizable [26,27]. In this article we entirely work with regions I and II, that is, restricting ourselves to $\alpha \geqslant 0$, where the line

$$\alpha_c(v_0) = \frac{1}{1 - 2v_0} \tag{3}$$

corresponds to $\mathcal{E}^{(2)} = 0$ and separates region I with a single virtual state and region II with a single bound state. To explore the Borromean states in the three-particle system, we focus on the transition between these two regions. For $\alpha < 0$, the two-particle subsystem supports either one virtual and one bound state (region III), or two bound states (region IV).

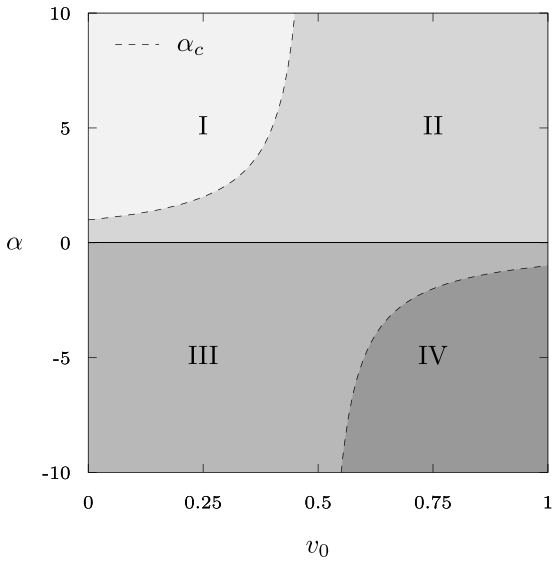

FIG. 1. The parameter space (α, v_0) of the two-body subsystems divided into four separate regions with respect to the number of bound and virtual states. From top-left to bottom-right: one virtual state (region I), one bound state (region II), one virtual and one bound state (region III), two bound states (region IV). The dashed line indicates $\alpha_c(v_0)$ given by Eq. (3).

B. Three-particle system

Next, we consider a three-body system in one dimension with two identical bosons (B) of mass M and one distinguishable particle (X) of mass m. We assume no interaction between the two bosons, while the BX subsystems interact via the potential $v(x)$, Eq. (2).

By eliminating the center-of-mass motion of the three-body BBX system, depicted in Fig. 2, we arrive at the stationary Schrödinger equation,

$$[H_0 + V_{21} + V_{31}]\psi^{(3)} = \mathcal{E}^{(3)}\psi^{(3)}, \tag{4}$$

for the three-particle wave function $\psi^{(3)}(x_1, y_{23})$, where the Hamiltonian of the free motion is given by

$$H_0 = -\frac{\alpha_x}{2}\frac{\mathrm{d}^2}{\mathrm{d}x_1^2} - \frac{\alpha_y}{2}\frac{\mathrm{d}^2}{\mathrm{d}y_{23}^2}, \tag{5}$$

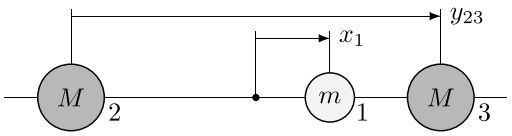

FIG. 2. The Jacobi coordinates x_1 and y_{23} for the one-dimensional three-particle (BBX) system. The dot shows the center of mass of two identical bosons, particles 2 and 3.

and both of its coefficients

$$\alpha_x = \frac{m+2M}{2(m+M)} \quad \text{and} \quad \alpha_y = \frac{2m}{m+M} \tag{6}$$

depend only on the mass ratio M/m. The two-body potential terms

$$V_{21} = v\left(x_1 + \frac{y_{23}}{2}\right) \quad \text{and} \quad V_{31} = v\left(x_1 - \frac{y_{23}}{2}\right) \tag{7}$$

for the BX subsystems are given by the function $v(x)$, Eq. (2), with the arguments being the relative distances between the respective particles B and X.

In this article we are interested in finding the Borromean states and their main features in our system. A three-body state is called *Borromean* if it is bound, while all of its two-body subsystems are unbound by themselves [5,6]. For our interaction potential $v(x)$, Eq. (2), the Borromean states should therefore lie in region I of the parameter space (α, v_0), displayed in Fig. 1, where there is no two-body bound state.

C. Faddeev equations

We employ the Faddeev equations [26,28,29] in order to calculate the bound-state spectrum and the wave functions of the BBX system. For a derivation of the explicit form of the Faddeev equations for our type of system, we refer to Appendix of Ref. [17]. In practice, all information is encapsulated in the set of one-dimensional integral equations

$$\varphi_\lambda(p,\mathcal{E}) = \sum_\nu \int_{\mathbb{R}} \frac{\mathrm{d}q}{2\pi} K_{\lambda\nu}(p,q,\mathcal{E})\varphi_\nu(q,\mathcal{E}) \tag{8}$$

for the functions $\varphi_\nu(p,\mathcal{E})$ with the kernel

$$K_{\lambda\nu}(p,q,\mathcal{E}) = \frac{g_\lambda(q+\beta p,\mathcal{E}_p)\, g_\nu^*(p+\beta q,\mathcal{E}_q)}{\mathcal{E} - \frac{1}{2}q^2 - \frac{1}{2}p^2 - \beta pq}\tau_\nu(\mathcal{E}_q) \tag{9}$$

and the shorthand notation

$$\beta = \frac{M}{M+m} \quad \text{and} \quad \mathcal{E}_p = \mathcal{E} - \frac{1}{2}\alpha_x\alpha_y p^2. \tag{10}$$

The functions $g_\nu(k,\mathcal{E})$ and $\tau_\nu(\mathcal{E})$ originate from the separable expansion for the off-shell t matrix of the BX subsystem, whereas the indices λ and ν denote the number of terms in this expansion. As shown in Appendix B, for the specific form of our interaction potential $v(x)$, Eq. (2), the separable expansion has exactly two terms, $\nu \in \{-,+\}$, and $g_\nu(k,\mathcal{E})$ and $\tau_\nu(\mathcal{E})$ can be derived analytically.

We solve Eq. (8) numerically, Appendix C, and obtain the energy $\mathcal{E}$ of three-body bound states together with their functions $\varphi_\nu(p,\mathcal{E})$. The latter can be used to construct the Faddeev component,

$$\Phi(k,p) = \sum_\nu g_\nu(k,\mathcal{E}_p)\tau_\nu(\mathcal{E}_p)\varphi_\nu(p,\mathcal{E}), \tag{11}$$

and finally, the wave function

$$\begin{aligned}\psi(p_1,k_{23}) = G_0(p_1,k_{23},\mathcal{E}) \\ \times\left[\Phi\left(-\alpha_x p_1 - \frac{\alpha_y}{2}k_{23}, -\frac{1}{2}p_1 + k_{23}\right)\right. \\ \left. + \Phi\left(-\alpha_x p_1 + \frac{\alpha_y}{2}k_{23}, -\frac{1}{2}p_1 - k_{23}\right)\right]\end{aligned} \tag{12}$$

of the three-body system in momentum space. Here,

$$G_0(p_1,k_{23},\mathcal{E}) = \frac{(2\pi)^2}{\mathcal{E} - \frac{1}{2}\alpha_x p_1^2 - \frac{1}{2}\alpha_y k_{23}^2} \tag{13}$$

is the Green function of the free three-body system, corresponding to the Hamiltonian H_0, Eq. (5).

In this way the wave function in position space can be obtained from the Fourier transform

$$\psi^{(3)}(x_1,y_{23}) = \int_{\mathbb{R}} \frac{\mathrm{d}p_1}{2\pi}\int_{\mathbb{R}} \frac{\mathrm{d}k_{23}}{2\pi} \mathrm{e}^{\mathrm{i}(p_1x_1 + k_{23}y_{23})}\psi^{(3)}(p_1,k_{23}) \tag{14}$$

of the wave function in momentum space.

III. BORROMEAN STATES

In this section we study the three-body spectrum of the BBX system and the conditions for the parameters α and v_0 under which the Borromean states exist, as well as the ground-state wave function and its geometric properties. Further, we examine the dependence of Borromean states on the mass ratio M/m.

The goal is to observe the behavior of the three-body BBX system while its BX subsystems undergo a transition from supporting exactly one bound state to supporting only a single virtual state. To do this we are tuning the parameters α and v_0 for both two-body interactions V_{21} and V_{31} simultaneously, so that both BX subsystems are identical at all times.

A. Existence and Borromean window

We start in parameter-region II, Fig. 1, at the point $(v_0 = 0.32, \alpha = 0)$, where the potential $v(x)$, Eq. (2), has only a single δ well and therefore the BX subsystem supports exactly one bound state. We confirm the correctness of our calculations by setting the mass ratio to $M/m = 22.2$, corresponding to a Cs-Li mixture [30,31], and reproducing the energy spectrum

$$\begin{aligned}\mathcal{E}_0^{(3)} &= 2.7515\ \mathcal{E}^{(2)} \\ \mathcal{E}_1^{(3)} &= 1.3604\ \mathcal{E}^{(2)} \\ \mathcal{E}_2^{(3)} &= 1.0525\ \mathcal{E}^{(2)}\end{aligned} \tag{15}$$

of three-body bound states reported previously in Ref. [32] and obtained with the Skorniakov-Ter-Martirosian method [33]. Here, $\mathcal{E}_0^{(3)}, \mathcal{E}_1^{(3)}$, and $\mathcal{E}_2^{(3)}$ denote the energies of the ground, first excited, and second excited three-body state, respectively, in units of the two-body energy $\mathcal{E}^{(2)}$.

Positive values for α introduce a repulsive barrier in the potential $v(x)$, Eq. (2). Therefore, increasing α pushes the two-body energy $\mathcal{E}^{(2)}$ of the single bound state in the BX subsystems closer to the threshold, $\mathcal{E}^{(2)} = 0$, which is reached

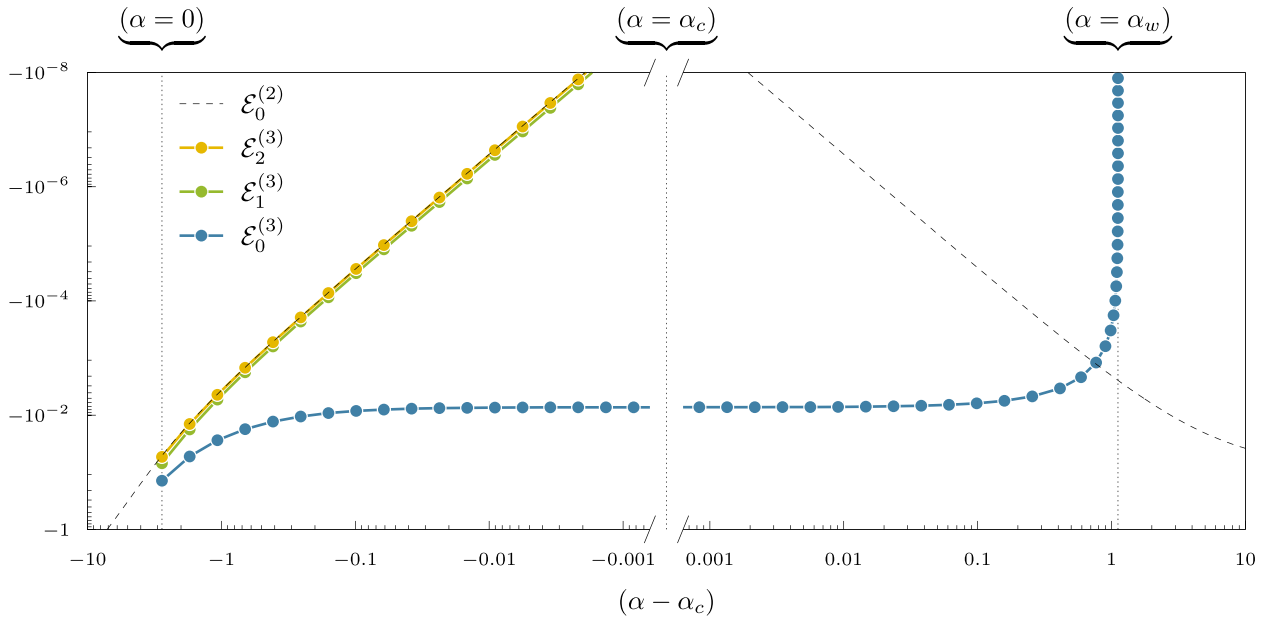

FIG. 3. Three-body spectrum as a function of the repulsion parameter α for the coupling constant $v_0 = 0.32$ and the mass ratio $M/m = 22.2$. The dashed line shows the energy $\mathcal{E}_0^{(2)}$ of the two-body bound state (left) or virtual state (right), whereas the dotted lines display the energies $\mathcal{E}_n^{(3)}$ of the three-body bound states. As α approaches α_c from below (left), the energies $\mathcal{E}_1^{(3)}$ and $\mathcal{E}_2^{(3)}$ of the excited three-body states follow the two-body energy described by the power law, Eq. (16), and vanish at $\alpha = \alpha_c$. On the contrary, the three-body ground state has a finite, negative energy $\mathcal{E}_0^{(3)}$ at $\alpha = \alpha_c$ and remains bound even for $\alpha > \alpha_c$ (right), until $\alpha = \alpha_w$. As for $\alpha > \alpha_c$, there is no two-body bound state, this three-body state is Borromean, and the interval $\alpha_c < \alpha < \alpha_w$ defines the Borromean window.

at $\alpha = \alpha_c$. For the corresponding BBX system, increasing the barrier strength α results in larger energies $\mathcal{E}_n^{(3)}$, i.e., weaker binding, for all three bound states, as displayed in Fig. 3. When α approaches α_c, only the energies $\mathcal{E}_1^{(3)}$ and $\mathcal{E}_2^{(3)}$ of the excited states vanish together with the energy $\mathcal{E}^{(2)}$, depicted by the dashed line. The linear behavior in the log-log scale of Fig. 3 suggests a power-law dependence, and in Appendix A we indeed find

$$\mathcal{E}^{(2)} \approx -\frac{1}{2}\left[\frac{v_0(1-2v_0)^2}{(1-v_0)^2+v_0^2}\right]^2 (\alpha - \alpha_c)^2 \qquad (16)$$

as the relative coupling strength of the barrier $\alpha \to \alpha_c$ and therefore $\mathcal{E}^{(2)} \to 0$. In sharp contrast, the three-body ground state does not dissociate at the two-body threshold. Instead, its energy $\mathcal{E}_0^{(3)}$ takes a finite, negative value at $\alpha = \alpha_c$, Fig. 3.

It is important to mention that the quadratic power law of Eq. (16) is very similar to the results proven in Ref. [13], where a one-dimensional two-body system is considered and the coupling strength of the full potential goes to zero.

By increasing α beyond α_c, we enter region I of Fig. 1, where the two-body systems become unbound and each only has one virtual state. Here, the BBX system is however able to retain the bound ground state. We emphasize that both BX subsystems are unbound, and hence the three-body state is Borromean. Moreover, we note that the energy $\mathcal{E}_0^{(3)}$ of this Borromean state as a function of α changes continuously at the point $\alpha = \alpha_c$. In addition, we observe from Fig. 3 that for even larger values of α, the Borromean state eventually disappears at $\alpha = \alpha_w$, above which there is no three-body bound state anymore. For $\alpha \to \alpha_w$, we numerically find that $\mathcal{E}_0^{(3)}$ follows the power law

$$\mathcal{E}_0^{(3)} \approx -0.001\,717\,5\,(\alpha_w - \alpha)^{1.0605}, \qquad (17)$$

with $\alpha_w = 3.895\,063\,3$. We emphasize that the fit given by Eq. (17) has a small relative error with respect to the data points, $|(\mathcal{E}_{\text{data}} - \mathcal{E}_{\text{fit}})/\mathcal{E}_{\text{data}}| \leqslant 10^{-2}$ for $9 \times 10^{-6} \leqslant (\alpha_w - \alpha) \leqslant 7 \times 10^{-4}$ including nine data points. Moreover, as shown in Fig. 3, the energy $\mathcal{E}_0^{(3)}$ is no longer smaller than the energy $\mathcal{E}^{(2)}$ of the corresponding virtual state in the two-body subsystem.

In summary, we find that for a given potential strength v_0 and mass ratio M/m, a Borromean state exists in the BBX system in the window $\alpha_c < \alpha < \alpha_w$. By determining α_c and α_w for multiple values of v_0, we identify an area in the parameter space (α, v_0), Fig. 1, where the Borromean state occurs, as depicted in Fig. 4. Here it becomes evident that a larger magnitude v_0 leads to a wider "Borromean window" (α_c, α_w) for α.

The numerical results presented in this section are checked for convergence by varying the number of discretization points for the momenta needed to solve Eq. (8). We have calculated the relative error of the three-body ground-state energy $\varepsilon_r = |(\mathcal{E}_N - \mathcal{E}_{N'})/\mathcal{E}_N|$ (for $N = 1536$ and $N' = 1280$) to be small ($\varepsilon_r \leqslant 10^{-3}$) in the threshold region $\alpha \approx \alpha_w$ and very small ($\varepsilon_r \leqslant 10^{-7}$) everywhere else. The larger error at the threshold is expected, because the wave function is very large and the calculations become very sensitive to the discretization at the small values of the momenta.

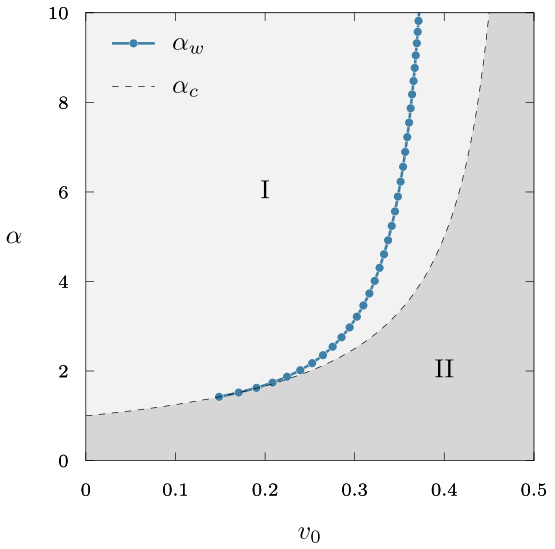

FIG. 4. Upper-left quadrant of Fig 1, displaying the parameter space (α, v_0). We highlight two curves: (i) the two-body threshold α_c, given by Eq. (3) and shown by dashed line, separates regions (I) and (II) with one virtual and one bound state in the BX subsystems, respectively. (ii) The three-body threshold α_w marks the line, displayed by blue dots, above which there is no three-body bound state. It generally depends on the mass ratio, here $M/m = 22.2$, and is determined numerically. Together, both lines define an area ("Borromean window") between the dotted and dashed curves in which our system has Borromean states.

B. Geometric properties

Studying the geometric properties of the three-body ground state gives us insight into its particle configuration. For that we calculate the wave function $\psi^{(3)}(x_1, y_{23})$ of the BBX system and present a contour plot of $|\psi^{(3)}(x_1, y_{23})|$ in Fig. 5 for three different values of the parameter α: $\alpha = 0$, (a), $\alpha = 2.11$, (b), and $\alpha = 3.84$, (c). To visualize the interaction potentials in both BX subsystems, we plot additionally the dashed lines $x_1 \pm y_{23}/2 = 1/2$ (purple) and $x_1 \pm y_{23}/2 = -1/2$ (red), describing the attractive and repulsive δ wells in $v(x)$, Eq. (2), respectively. In addition, we calculate the expectation values $\langle x_1 \rangle$ and $\langle y_{23} \rangle$, as well as the standard deviations σ_{x_1} and $\sigma_{y_{23}}$ as functions of α, with

$$\sigma_z = \sqrt{\langle z^2 \rangle - \langle z \rangle^2}, \tag{18}$$

and display them in Figs. 6(a) and 6(b), accordingly.

For zero repulsion in the interaction ($\alpha = 0$), Fig. 5(a) shows that the wave function $|\psi^{(3)}(x_1, y_{23})|$ is point symmetric with respect to its expectation values $\langle x_1 \rangle = 1/2$ and $\langle y_{23} \rangle = 0$. Since y_{23} is the distance between the identical bosonic particles, Fig. 2, the wave function $\psi^{(3)}(x_1, y_{23})$ is symmetric in this coordinate, i.e., $\psi^{(3)}(x_1, -y_{23}) = \psi^{(3)}(x_1, y_{23})$, giving rise to $\langle y_{23} \rangle = 0$ for all parameters. Apart from the shift by $1/2$ in x_1 direction, this result coincides with the one found previously [32] for the same three-body system but with the single contact interaction being centered.

Next, we increase the repulsion by setting $\alpha = 2.11$, a bit below $\alpha_c = 2.78$, and present the resulting wave function in Fig. 5(b). Here we have a shift of the expected position $\langle x_1 \rangle = 2.31$ of the distinguishable particle, whereas $\langle y_{23} \rangle = 0$, as shown in Fig. 6(a). Moreover, the wave function becomes broader compared to the case with $\alpha = 0$, Fig. 5(a), which is also indicated by the scale of $|\psi(x_1, y_{23})|$ as well as the standard deviations σ_{x_1} and $\sigma_{y_{23}}$, presented in Fig. 6(b). The result also agrees with the fact that the ground-state energy $\mathcal{E}_0^{(3)}$ at $\alpha = 2.11$ is smaller by about one order in comparison with $\mathcal{E}_0^{(3)}$ at $\alpha = 0$, as displayed by Fig. 3.

Now increasing α to the value slightly below α_w, which identifies the Borromean three-body threshold, Fig. 5(c), the wave function $\psi(x_1, y_{23})$ shows that the distinguishable particle moves on average even further away, $\langle x_1 \rangle = 19.5$, from the center of mass of the identical particles, whereas $\langle y_{23} \rangle = 0$, Fig. 6(a). In addition, the wave function becomes again broader and extremely delocalized with very weak binding energy $\mathcal{E}_0^{(3)}$ as $\alpha \to \alpha_w$, Fig. 3, before the Borromean ground state dissociates completely. This observation is in line with both standard deviations σ_{x_1} and $\sigma_{y_{23}}$ becoming very large when α approaches α_w, Fig. 6(b).

It is important to note that the wave function continuously changes as the function of α throughout Figs. 5(a), 5(b) and 5(c), as do the expectation values presented in Fig. 6.

C. Dependence on the mass ratio

Finally, we analyze the dependence of the Borromean three-body energy on the mass ratio M/m. This is shown in Fig. 7. Here we choose α to be just slightly above α_c, i.e., we are just inside the Borromean window, where the Borromean states are relatively deeply bound. Nevertheless, we see that for smaller mass ratios, the binding energy of the Borromean ground state (blue line) quickly approaches zero. On the other hand, as the mass ratio increases, this Borromean state becomes more strongly bound. Moreover, when the mass ratio is sufficiently large ($M/m \gtrsim 600$), a second (excited) Borromean state appears, as depicted by a green line. We note that the energy $\mathcal{E}^{(3)}$ is expressed in units of $\hbar^2/(\mu a^2)$ with the reduced mass μ. Overall, for larger mass ratios the three-body states become more bound, and the Borromean states appear one by one.

To trace back the origin of the second Borromean state, we analyze the three-body spectrum for different values of α and M/m, as demonstrated in Fig. 8. In Fig. 8(a) we choose $M/m = 0.2$ and we cannot find a Borromean state. There is just a single non-Borromean bound state for $\alpha < \alpha_c$. That is similar to the case of when the subsystems have a zero-range interaction, then the three-body system does not support more than one bound state for $M/m \leqslant 1$ [34]. At an intermediate value of the mass ratio, e.g., $M/m = 22.2$ in Fig. 3, we clearly see the three-body ground state in the Borromean region, $\alpha_c < \alpha < \alpha_w$. Finally, for $M/m = 720$, Fig. 8(b), the ground state is quite deeply bound and we see the second state (green line) in the Borromean window. Again, the energy of all three-body bound states changes smoothly as a function of α when crossing the value $\alpha = \alpha_c$.

IV. EXPERIMENTAL VERIFICATION

For an experimental verification of our theoretical predictions we suggest a system of two parallel one-dimensional

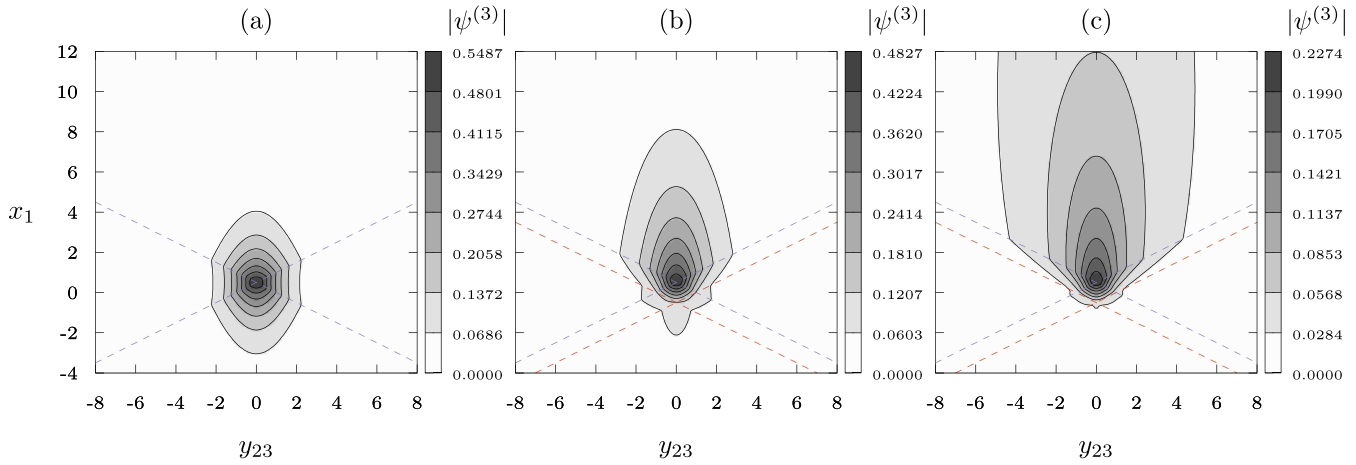

FIG. 5. Contour plots of the Borromean ground-state wave function $|\psi^{(3)}(x_1, y_{23})|$ in position space spanned by the Jacobi coordinates x_1 and y_{23}, Fig. 2, for three different values of the repulsion parameter: $\alpha = 0$ (a), $\alpha = 2.11$ (b), $\alpha = 3.84$ (c), as well as $v_0 = 0.32$ and $M/m = 22.2$. With increasing α, the wave function starts to become increasingly skewed towards the positive x_1 direction, whereas it remains symmetric in y_{23} direction. Similarly to the energy spectrum shown in Fig. 3, this trend is continuous and no sudden change occurs when the state becomes Borromean. For all values of α, the derivative of the wave function jumps at the positions of the attractive (repulsive) contact interactions, highlighted by purple (red) dashed lines.

tube-shaped traps [24]. The first tube contains two heavy dipolar particles of mass M, whereas the second one contains a dipolar particle of mass m. When the dipole vectors

$$\mathbf{D} = D[\cos(\theta)\cos(\phi),\ \cos(\theta)\sin(\phi),\ \sin(\theta)] \tag{19}$$

of these three particles are identical and aligned by an external field, the interaction potential between heavy and light particles reads [24,25]

$$V_{\mathrm{BX}}(x) = \frac{D^2}{d^3}\frac{x^2 + 1 - 3\cos^2(\theta)[x\cos(\phi) + \sin(\phi)]^2}{(x^2+1)^{5/2}}. \tag{20}$$

Here x is the dimensionless distance between particles along the tubes in terms of the distance d between two tubes.

The interaction potential $V_{\mathrm{BB}}(x)$ between the two identical heavy particles inside the same tube is given by

$$V_{\mathrm{BB}}(x) = \frac{D^2}{d^3}\frac{1 - 3\cos^2(\theta)\cos^2(\phi)}{|x|^3} \tag{21}$$

and can be set to zero at $\cos^2(\theta)\cos^2(\phi) = 1/3$. We emphasize that the interaction potential $V_{\mathrm{BX}}(x)$ between two dipoles in different tubes has attractive and repulsive parts and is not symmetric, similar to our BX potential, Eq. (2). Moreover, as shown in Ref. [25], the potential $V_{\mathrm{BX}}(x)$ supports a bound state for $\cos(2\theta) \geqslant 1/3$ and no bound state for $\cos(2\theta) < 1/3$, under the condition that $\cos^2(\theta)\cos^2(\phi) = 1/3$. As a result, by changing the direction of the dipole moment $\mathbf{D}$ with respect to the tube, one can realize a smooth transition between these two cases, that is, the transition between regions I and II shown in Fig. 1. Hence, this experimental scheme based on dipolar particles [25,35] allows one to realize the one-dimensional Borromean three-particle states predicted and studied in this article.

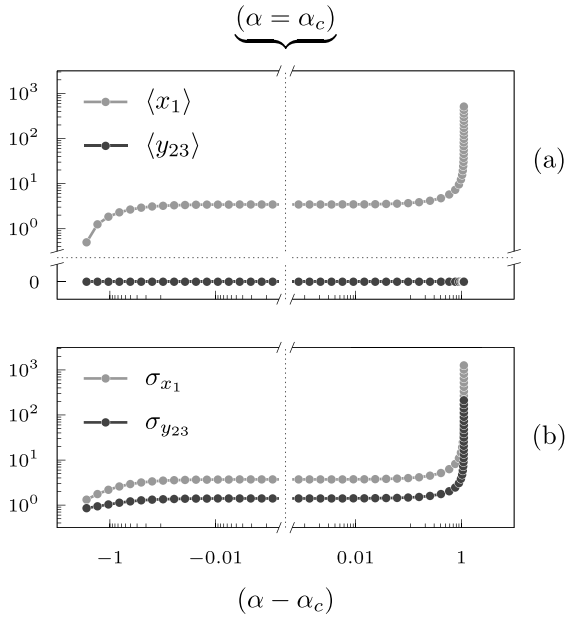

FIG. 6. The expectation values $\langle x_1 \rangle$, $\langle y_{23} \rangle$ (a) and the standard deviations σ_{x_1}, $\sigma_{y_{23}}$ (b), Eq. (18), as functions of α. Top: With increasing α, also $\langle x_1 \rangle$ increases, meaning that the distinguishable particle is found on average further away from the center of mass of the two bosons. Close to the dissociation point α_w, $\langle x_1 \rangle$ becomes very large. As the other two particles are identical, $\langle y_{23} \rangle$ remains zero for all values of α. Bottom: Both standard deviations σ_{x_1}, $\sigma_{y_{23}}$ grow with increasing α. Overall, the effect is stronger for the x_1 coordinate and for both directions strongly enhanced close to the dissociation point α_w where the three-body state becomes very dilute.

V. CONCLUSION

In this article we have investigated Borromean states in a three-body BBX system confined in one dimension, provided there is no interaction in the BB subsystem and each BX subsystem supports only a single virtual state. By solving

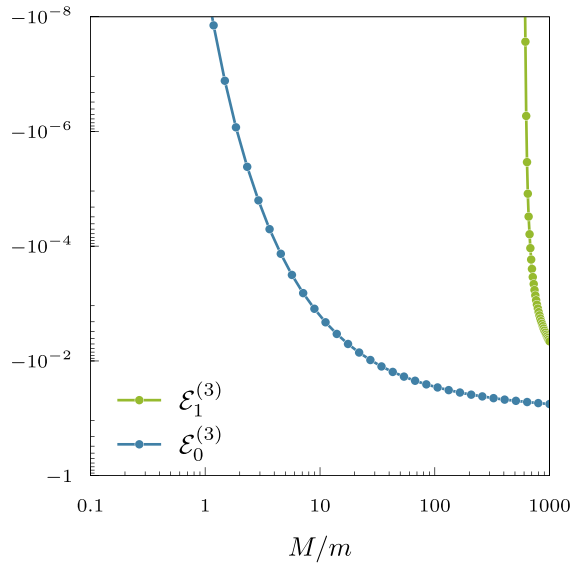

FIG. 7. Three-body spectrum as a function of the mass ratio M/m and with coupling constant $v_0 = 0.32$. We choose the repulsion parameter α just above α_c, i.e., inside the Borromean window, Fig. 4, and therefore the displayed states are Borromean. With increasing mass ratio, the system goes from supporting zero, to one, and to two Borromean bound states.

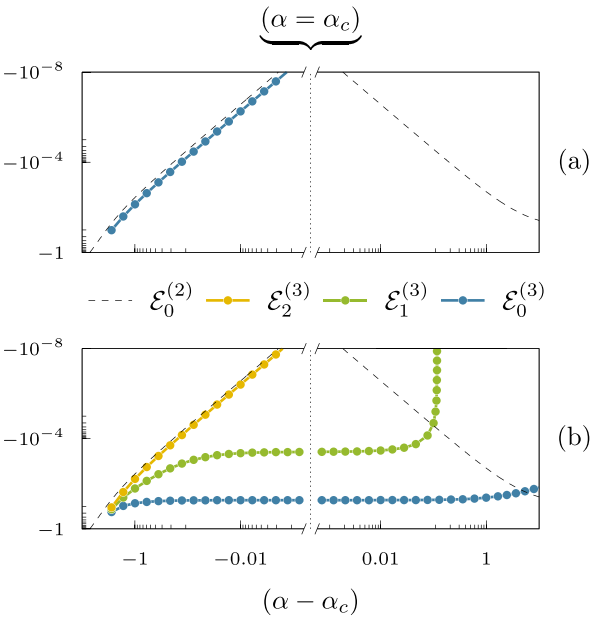

FIG. 8. Three-body spectrum as a function of α with constant $v_0 = 0.32$ for the mass ratios $M/m = 0.2$ (a) and $M/m = 720$ (b). Top: The BBX systems supports only a single three-body bound state for $\alpha < \alpha_c$ and it dissociates at $\alpha = \alpha_c$, leading to no Borromean state for the small mass ratio. Bottom: For the much larger mass ratio, the three-body system supports many bound states for $\alpha < \alpha_c$. Here, only the first three bound states with the lowest energies are presented. The two deepest bound states remain bound also for $\alpha > \alpha_c$ and are hence Borromean states.

the Faddeev equations numerically, we have calculated the spectrum and the corresponding wave functions of the BBX system. We have demonstrated the existence of Borromean states in our system and, for a given mass ratio, identified an area in the parameter space where these states occur. Further, we have found that the number of Borromean states and their binding energies strongly depend on the mass ratio of the two particles types. In addition, we have shown that in all cases these novel states originate from ordinary bound ones with the lowest three-body binding energies. Finally, we have proposed an experimental scheme based on dipolar particles in one-dimensional tubes to verify our theoretical predictions.

ACKNOWLEDGMENTS

We thank A. Volosniev and P. Belov for fruitful discussions and advice. The work of L.H. is gratefully supported by the RIKEN special postdoctoral researcher program. The authors gratefully acknowledge the scientific support and HPC resources provided by the German Aerospace Center (DLR). The HPC system CARA is partially funded by "Saxon State Ministry for Economic Affairs, Labour and Transport" and "Federal Ministry for Economic Affairs and Climate Action."

APPENDIX A: BX SUBSYSTEM

In this Appendix we derive the transcendental equation for the spectrum of the BX subsystem. Moreover, we discuss the number of solutions as a function of α and derive the asymptotic behavior of the two-body energy near the threshold $\alpha \to \alpha_c$.

We start from the stationary Schrödinger equation,

$$\left[-\frac{1}{2}\frac{\mathrm{d}^2}{\mathrm{d}x^2} + v(x)\right]\psi^{(2)}(x) = \mathcal{E}^{(2)}\psi^{(2)}(x), \tag{A1}$$

where the two-body interaction potential $v(x)$ is given by the potential

$$v(x) = -v_0\left[\delta\left(x - \tfrac{1}{2}\right) - \alpha\delta\left(x + \tfrac{1}{2}\right)\right] \tag{A2}$$

with positive v_0.

With κ defined as $\mathcal{E}^{(2)} = \kappa^2/2$, the solution of Eq. (A1) can be written in the form

$$\psi^{(2)}(x) = \begin{cases} A\mathrm{e}^{\mathrm{i}\kappa x} + A'\mathrm{e}^{-\mathrm{i}\kappa x}, & x < -\frac{1}{2} \\ B\mathrm{e}^{\mathrm{i}\kappa x} + B'\mathrm{e}^{-\mathrm{i}\kappa x}, & -\frac{1}{2} < x < \frac{1}{2} \\ C\mathrm{e}^{\mathrm{i}\kappa x} + C'\mathrm{e}^{-\mathrm{i}\kappa x}, & \frac{1}{2} < x, \end{cases} \tag{A3}$$

where A, A', B, B', C, and C' are constants.

To determine them, we first incorporate the outgoing-wave boundary condition [36], that is, $A = C' = 0$. Next, we require the wave function to be continuous at $x = -\frac{1}{2}$ and $x = \frac{1}{2}$ and arrive at two conditions,

$$A'\mathrm{e}^{\mathrm{i}\kappa/2} = B\mathrm{e}^{-\mathrm{i}\kappa/2} + B'\mathrm{e}^{\mathrm{i}\kappa/2}, \tag{A4}$$

$$B\mathrm{e}^{\mathrm{i}\kappa/2} + B'\mathrm{e}^{-\mathrm{i}\kappa/2} = C\mathrm{e}^{\mathrm{i}\kappa/2}. \tag{A5}$$

Integrating the Schrödinger equation (A1) on the intervals $x \in [-\frac{1}{2} - \epsilon, -\frac{1}{2} + \epsilon]$ and $x \in [\frac{1}{2} - \epsilon, \frac{1}{2} + \epsilon]$, and then taking the limit $\epsilon \to 0$, gives us expressions for the jump of the

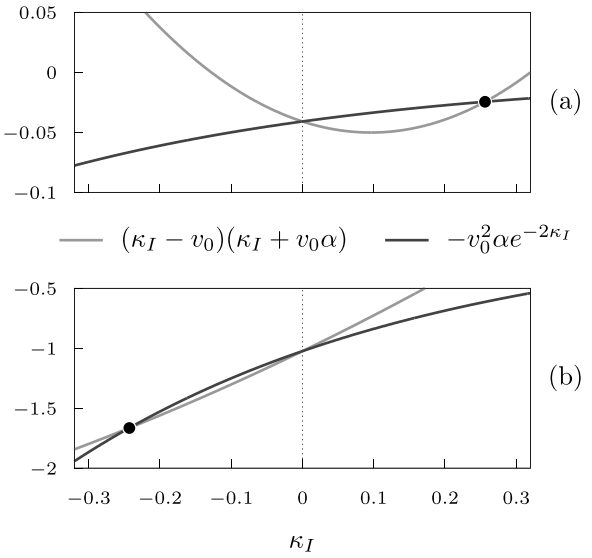

FIG. 9. The left- and right-hand sides of the transcendental equation (A8) as functions of κ_I with $v_0 = 0.32$. We look for solutions $\kappa_I \neq 0$. In subfigure (a) $\alpha = 0.4$ and the intersection of these lines is marked by a dot and occurs for $\kappa_I > 0$, corresponding to the bound state. In subfigure (b) $\alpha = 10$, the intersection occurs for $\kappa_I < 0$ and corresponds to the virtual state.

derivative of the wave function at $x = -\frac{1}{2}$ and $x = \frac{1}{2}$, respectively. These expressions yield the two additional conditions

$$A'\left(1 + 2i\frac{v_0\alpha}{\kappa}\right)e^{i\kappa/2} + Be^{-i\kappa/2} - B'e^{i\kappa/2} = 0 \tag{A6}$$

$$-Be^{i\kappa/2} + B'e^{-i\kappa/2} + C\left(1 - 2i\frac{v_0}{\kappa}\right)e^{i\kappa/2} = 0. \tag{A7}$$

The system of four linear equations (A4)–(A7) for the coefficients A', B, B', and C has nontrivial solutions only if the determinant of this system equals zero, giving rise to a transcendental equation for $\kappa = \kappa_R + i\kappa_I$. By setting $\kappa_R = 0$, we restrict the possible solutions to virtual ($\kappa_I < 0$) and bound ($\kappa_I > 0$) states and obtain the transcendental equation

$$(\kappa_I - v_0)(\kappa_I + v_0\alpha) = -v_0^2\alpha e^{-2\kappa_I} \tag{A8}$$

for κ_I.

We are not interested in the trivial solution $\kappa_I = 0$ of Eq. (A8). In Fig. 9 both the left (gray line) and right (black line) sides of Eq. (A8) are depicted as a function of κ_I. We see that for $\alpha > 0$ there is one nontrivial solution (black dot). Whether this root is located on the positive or negative κ_I axis depends on the difference of the derivatives of the left- and right-hand sides of Eq. (A8) at $\kappa_I = 0$, that is, $v_0(\alpha - 1) - 2v_0^2\alpha = v_0(\alpha - 1 - 2v_0\alpha)$. This difference vanishes for

$$\alpha = \alpha_c = \frac{1}{1 - 2v_0}. \tag{A9}$$

In this way, for $0 < \alpha < \alpha_c$ there is only one bound state (with $\kappa_I > 0$) in the BX subsystem, whereas for $0 < \alpha_c < \alpha$, the subsystem supports only one virtual state (with $\kappa_I < 0$). In the case $\alpha < 0$, there are one bound and one virtual state for $\alpha_c < \alpha < 0$ and two bound states for $\alpha < \alpha_c < 0$. All these cases are summarized in the parameter space of the BX subsystem, Fig. 1.

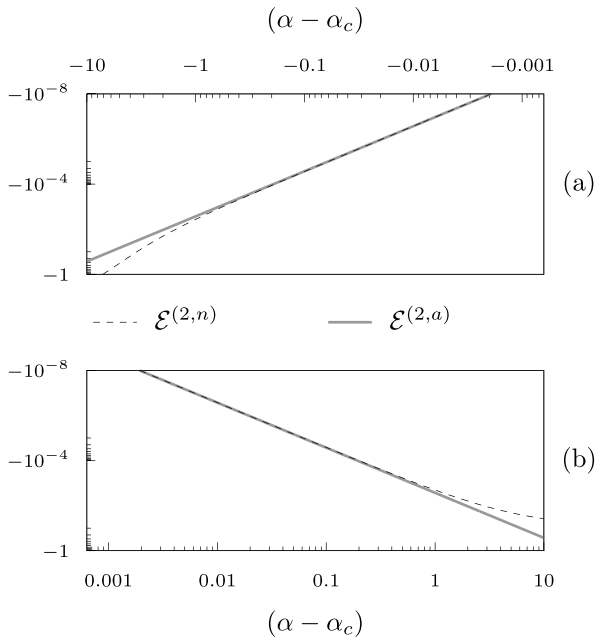

FIG. 10. Comparison of the two-body energy $\mathcal{E}^{(2,a)}$, given by the asymptotic expansion, Eq. (A14), to $\mathcal{E}^{(2,n)}$ obtained as the numerical solution of the transcendental equation (A8). Subfigure (a) shows the solution for the bound state with $\alpha < \alpha_c$, whereas subfigure (b) displays the solution for the virtual state with $\alpha_c < \alpha$.

In addition, we now derive the analytical formula for the nontrivial solution of Eq. (A8) as $\alpha \to \alpha_c$. In this limit the nontrivial root $\kappa_I \to 0$. Therefore, we can use the asymptotic expansion

$$e^{-2\kappa_I} = 1 - 2\kappa_I + 2\kappa_I^2 + \mathcal{O}(\kappa_I^3) \tag{A10}$$

in Eq. (A8) and solve the resulting equation for $\kappa_I \neq 0$, to arrive at

$$\kappa_I(\alpha) \approx v_0\frac{1 + \alpha(2v_0 - 1)}{1 + 2v_0^2\alpha}. \tag{A11}$$

Next, we expand α around α_c to the first order and obtain

$$\kappa_I(\alpha) \approx c_1(\alpha - \alpha_c) \tag{A12}$$

with the coefficient

$$c_1 = -\frac{v_0(1 - 2v_0)^2}{(1 - v_0)^2 + v_0^2}. \tag{A13}$$

As a result, we obtain the approximate behavior

$$\mathcal{E}^{(2)}(\alpha) = -\frac{1}{2}\kappa_I^2 \approx -\frac{c_1^2}{2}(\alpha - \alpha_c)^2 \tag{A14}$$

of the two-body energy as $\alpha \to \alpha_c$. The asymptotic approximation is compared to the exact numerical solution in Fig. 10.

APPENDIX B: SEPARABLE EXPANSION

In this Appendix we derive the analytical form of the separable expansion [26] for the two-body t matrix, corresponding to the two-body potential $v(x)$, Eq. (2).

We expand the t matrix in separable terms,

$$t(k,k',\mathcal{E}) = \sum_{\nu} \tau_\nu(\mathcal{E}) g^*_\nu(k,\mathcal{E}) g_\nu(k',\mathcal{E}), \tag{B1}$$

with

$$\tau_\nu(\mathcal{E}) = \frac{\eta_\nu(\mathcal{E})}{\eta_\nu(\mathcal{E})-1}, \tag{B2}$$

where the functions $\eta_\nu(k,\mathcal{E})$ and $g_\nu(\mathcal{E})$ are determined by the integral equation

$$\int_{\mathbb{R}} \frac{\mathrm{d}k'}{2\pi} \frac{v(k,k')}{\mathcal{E}-\frac{1}{2}k'^2} g_\nu(k',\mathcal{E}) = \eta_\nu(\mathcal{E}) g_\nu(k,\mathcal{E}). \tag{B3}$$

Here,

$$v(k,k') = \int_{\mathbb{R}} \mathrm{d}x\, v(x)\, \mathrm{e}^{-\mathrm{i}(k-k')x} \tag{B4}$$

is the momentum representation of the two-body interaction potential $v(x)$ and the functions $g_\nu(k,\mathcal{E})$ are orthogonal and normalized according to the condition

$$\int_{\mathbb{R}} \frac{\mathrm{d}k}{2\pi} \frac{g_\nu(k,\mathcal{E})\, g^*_{\nu'}(k,\mathcal{E})}{\mathcal{E}-\frac{1}{2}k^2} = -\delta_{\nu,\nu'}. \tag{B5}$$

By inserting the potential defined in Eq. (2) into Eq. (B4), we find

$$v(k,k') = -v_0[e^{-\mathrm{i}(k-k')/2} - \alpha\, \mathrm{e}^{\mathrm{i}(k-k')/2}], \tag{B6}$$

resulting in a separable kernel of the integral equation (B3). This allows us to rewrite Eq. (B3) in the form

$$-v_0[\mathrm{e}^{-\mathrm{i}k/2} G^{(+)}_\nu(\mathcal{E}) - \alpha\, \mathrm{e}^{\mathrm{i}k/2} G^{(-)}_\nu(\mathcal{E})] = \eta_\nu(\mathcal{E}) g_\nu(k,\mathcal{E}), \tag{B7}$$

where

$$G^{(\pm)}_\nu(\mathcal{E}) = \int_{\mathbb{R}} \frac{\mathrm{d}k'}{2\pi} \frac{\mathrm{e}^{\pm \mathrm{i}k'/2}}{\mathcal{E}-\frac{1}{2}k'^2} g_\nu(k',\mathcal{E}) \tag{B8}$$

are single-argument functions of the energy $\mathcal{E}$.

In order to determine $G^{(\pm)}_\nu(\mathcal{E})$, we insert the function $g_\nu(k,\mathcal{E})$ given by Eq. (B7) into Eq. (B8) and obtain

$$\left(1+\frac{v_0}{\eta_\nu}\mathcal{A}\right) G^{(+)}_\nu - \frac{v_0\alpha}{\eta_\nu}\mathcal{B} G^{(-)}_\nu = 0 \tag{B9}$$

$$\frac{v_0}{\eta_\nu}\mathcal{B}^* G^{(+)}_\nu + \left(1-\frac{v_0\alpha}{\eta_\nu}\mathcal{A}\right) G^{(-)}_\nu = 0 \tag{B10}$$

with

$$\mathcal{A} = \int_{\mathbb{R}} \frac{\mathrm{d}k'}{2\pi} \frac{1}{\mathcal{E}-\frac{1}{2}k'^2} = -\frac{1}{\sqrt{-2\mathcal{E}}} \tag{B11}$$

and

$$\mathcal{B} = \int_{\mathbb{R}} \frac{\mathrm{d}k'}{2\pi} \frac{\mathrm{e}^{\mathrm{i}k'}}{\mathcal{E}-\frac{1}{2}k'^2} = -\frac{1}{\sqrt{-2\mathcal{E}}} \mathrm{e}^{-\sqrt{-2\mathcal{E}}}, \tag{B12}$$

valid for $\mathcal{E} < 0$.

The system of algebraic equations (B9)–(B10) for $G^{(-)}_\nu$ and $G^{(+)}_\nu$ has nontrivial solutions only when the determinant of this system is zero, that is,

$$(\eta_\nu + v_0\mathcal{A})(\eta_\nu - v_0\alpha\mathcal{A}) + v_0^2\alpha|\mathcal{B}|^2 = 0, \tag{B13}$$

resulting in two eigenvalues

$$\eta_\pm(\mathcal{E}) = \frac{v_0}{2\sqrt{-2\mathcal{E}}}[1-\alpha \pm \mathcal{S}(\mathcal{E})] \tag{B14}$$

with

$$\mathcal{S}(\mathcal{E}) = \sqrt{(1-\alpha)^2 + 4\alpha(1-e^{-2\sqrt{-2\mathcal{E}}})}. \tag{B15}$$

Finally, using Eq. (B7) together with the normalization condition Eq. (B5), we obtain the expression

$$g_\nu(k,\mathcal{E}) = \frac{\frac{v_0}{\eta_\nu}\left|\frac{\eta_\nu}{v_0}\right|(-2\mathcal{E})^{1/4}}{\sqrt{\mathrm{e}^{2\sqrt{-2\mathcal{E}}}\mathcal{P}^2_\nu(\mathcal{E}) - 2\mathcal{P}_\nu(\mathcal{E}) + 1}} \times [\mathrm{e}^{\sqrt{-2\mathcal{E}}}\mathcal{P}_\nu(\mathcal{E})\mathrm{e}^{\mathrm{i}k/2} - \mathrm{e}^{-\mathrm{i}k/2}] \tag{B16}$$

with

$$\mathcal{P}_\nu(\mathcal{E}) = \left(1-\frac{\eta_\nu}{v_0}\sqrt{-2\mathcal{E}}\right) = \frac{\alpha \mathrm{e}^{-2\sqrt{-2\mathcal{E}}}}{\left(\frac{\eta_\nu}{v_0}\sqrt{-2\mathcal{E}}+\alpha\right)} \tag{B17}$$

for the corresponding eigenfunctions, where we used Eq. (B13) in the second step.

APPENDIX C: NUMERICS

In this Appendix we discuss our approach for the numerical solution of the integral Eq. (8). We use discrete momenta p_i and q_j with the indices $i, j \in \{0,\ldots,N-1\}$, with N being the number of discretization points, to define the vector elements

$$[\varphi_\lambda(\mathcal{E})]_i = \varphi_\lambda(p_i,\mathcal{E}) \tag{C1}$$

and the matrix elements

$$\left[\tilde{K}_{\lambda\nu}(\mathcal{E})\right]_{ij} = \frac{w_j}{2\pi} K_{\lambda\nu}(p_i,q_j,\mathcal{E}), \tag{C2}$$

respectively. The integral weights w_j depend on the exact form of the discretization. We use the Gauss-Legendre quadrature rule [37,38]. The indices λ and ν label the terms from the separable expansion given in Eq. (B1). In practice, the sum over ν in Eq. (8) needs to be finite or truncated. In the case of the two-body potential, Eq. (2), we have exactly two terms. The integral equation now takes the form of an

eigenvalue problem,

$$\underbrace{\begin{bmatrix}\varphi_0\\ \varphi_1\end{bmatrix}}_{=\mathbf{v}} = \pm \underbrace{\begin{bmatrix}\tilde{K}_{00} & \tilde{K}_{01}\\ \tilde{K}_{10} & \tilde{K}_{11}\end{bmatrix}}_{=\mathbf{W}} \begin{bmatrix}\varphi_0\\ \varphi_1\end{bmatrix}, \tag{C3}$$

with fixed eigenvalue $+1$ (-1) for bosons (fermions). Equation (C3) has a solution when

$$\det[\pm\mathbf{W}(\mathcal{E}) - \mathbb{I}] = 0 \tag{C4}$$

is fulfilled. The determinant in Eq. (C4) is calculated for a range of energy values $\mathcal{E}$, and each zero point of the determinant corresponds to an eigenenergy $\mathcal{E}^{(3)}$ of the three-body spectrum of Eq. (4).

To find the wave function, we calculate the eigenvector $\mathbf{v}(\mathcal{E}^{(3)})$ of the matrix $\mathbf{W}(\mathcal{E}^{(3)})$ for the corresponding eigenenergy $\mathcal{E}^{(3)}$. From the subvectors $\varphi_\nu(\mathcal{E}^{(3)})$ of the eigenvector $\mathbf{v}(\mathcal{E}^{(3)})$ we can get the Faddeev component from its separable terms via Eq. (11). Finally, we use Eq. (12) to obtain the wave function in momentum space.

[1] D. Blume, Few-body physics with ultracold atomic and molecular systems in traps, Rep. Prog. Phys. **75**, 046401 (2012).

[2] E. Nielsen, D. Fedorov, A. Jensen, and E. Garrido, The three-body problem with short-range interactions, Phys. Rep. **347**, 373 (2001).

[3] J.-M. Richard, The nonrelativistic three-body problem for baryons, Phys. Rep. **212**, 1 (1992).

[4] E. Braaten and H.-W. Hammer, Universality in few-body systems with large scattering length, Phys. Rep. **428**, 259 (2006).

[5] M. Zhukov, B. Danilin, D. Fedorov, J. Bang, I. Thompson, and J. Vaagen, Bound state properties of Borromean halo nuclei: 6He and 11Li, Phys. Rep. **231**, 151 (1993).

[6] P. Naidon and S. Endo, Efimov physics: A review, Rep. Prog. Phys. **80**, 056001 (2017).

[7] J. Goy, J.-M. Richard, and S. Fleck, Weakly bound three-body systems with no bound subsystems, Phys. Rev. A **52**, 3511 (1995).

[8] V. Efimov, Energy levels arising from resonant two-body forces in a three-body system, Phys. Lett. B **33**, 563 (1970).

[9] V. Efimov, Energy levels of three resonantly interacting particles, Nucl. Phys. A **210**, 157 (1973).

[10] A. S. Jensen, K. Riisager, D. V. Fedorov, and E. Garrido, Structure and reactions of quantum halos, Rev. Mod. Phys. **76**, 215 (2004).

[11] K. Riisager, Halos and related structures, Phys. Scr. **T152**, 014001 (2013).

[12] L. Moschini, F. Pérez-Bernal, and A. Vitturi, Bound and unbound nuclear systems at the drip lines: A one-dimensional model, J. Phys. G: Nucl. Part. Phys. **43**, 045112 (2016).

[13] B. Simon, The bound state of weakly coupled Schrödinger operators in one and two dimensions, Ann. Phys. **97**, 279 (1976).

[14] A. G. Volosniev, D. V. Fedorov, A. S. Jensen, and N. T. Zinner, Occurrence conditions for two-dimensional Borromean systems, Eur. Phys. J. D **67**, 95 (2013).

[15] A. G. Volosniev, D. V. Fedorov, A. S. Jensen, and N. T. Zinner, Borromean ground state of fermions in two dimensions, J. Phys. B: At., Mol. Opt. Phys. **47**, 185302 (2014).

[16] S. Moroz, J. P. D'Incao, and D. S. Petrov, Generalized Efimov effect in one dimension, Phys. Rev. Lett. **115**, 180406 (2015).

[17] L. Happ, M. Zimmermann, and M. A. Efremov, Universality of excited three-body bound states in one dimension, J. Phys. B: At., Mol. Opt. Phys. **55**, 015301 (2022).

[18] I. Bloch, Ultracold quantum gases in optical lattices, Nat. Phys. **1**, 23 (2005).

[19] I. Bloch, J. Dalibard, and W. Zwerger, Many-body physics with ultracold gases, Rev. Mod. Phys. **80**, 885 (2008).

[20] E. Timmermans, P. Tommasini, M. Hussein, and A. Kerman, Feshbach resonances in atomic Bose–Einstein condensates, Phys. Rep. **315**, 199 (1999).

[21] C. Chin, R. Grimm, P. Julienne, and E. Tiesinga, Feshbach resonances in ultracold gases, Rev. Mod. Phys. **82**, 1225 (2010).

[22] V. Dunjko, M. G. Moore, T. Bergeman, and M. Olshanii, Confinement-induced resonances, in *Advances in Atomic, Molecular, and Optical Physics*, Advances In Atomic, Molecular, and Optical Physics Vol. 60, edited by E. Arimondo, P. Berman, and C. Lin (Academic Press, 2011), Chap. 10, pp. 461–510.

[23] C. H. Greene, P. Giannakeas, and J. Pérez-Ríos, Universal few-body physics and cluster formation, Rev. Mod. Phys. **89**, 035006 (2017).

[24] N. T. Zinner, B. Wunsch, I. B. Mekhov, S.-J. Huang, D.-W. Wang, and E. Demler, Few-body bound complexes in one-dimensional dipolar gases and nondestructive optical detection, Phys. Rev. A **84**, 063606 (2011).

[25] A. G. Volosniev, J. R. Armstrong, D. V. Fedorov, A. S. Jensen, M. Valiente, and N. T. Zinner, Bound states of dipolar bosons in one-dimensional systems, New J. Phys. **15**, 043046 (2013).

[26] A. G. Sitenko, *Scattering Theory*, 1st ed., Springer Series in Nuclear and Particle Physics (Springer, Berlin, Heidelberg, 2012).

[27] R. G. Newton, *Scattering Theory of Waves and Particles*, 2nd ed., Theoretical and Mathematical Physics (Springer, Berlin, Heidelberg, 2014).

[28] L. D. Faddeev, Scattering theory for a three-particle system, Zh. Eksp. Teor. Fiz. **39**, 1459 (1960) [Sov. Phys. JETP **12**, 1014 (1961)].

[29] J. S. Ball, J. C. Y. Chen, and D. Y. Wong, Faddeev equations for atomic problems and solutions for the (e, h) system, Phys. Rev. **173**, 202 (1968).

[30] R. Pires, J. Ulmanis, S. Häfner, M. Repp, A. Arias, E. D. Kuhnle, and M. Weidemüller, Observation of Efimov resonances in a mixture with extreme mass imbalance, Phys. Rev. Lett. **112**, 250404 (2014).

[31] S.-K. Tung, K. Jiménez-García, J. Johansen, C. V. Parker, and C. Chin, Geometric scaling of Efimov states in a ^{6}Li – ^{133}Cs mixture, Phys. Rev. Lett. **113**, 240402 (2014).

[32] L. Happ, M. Zimmermann, S. I. Betelu, W. P. Schleich, and M. A. Efremov, Universality in a one-dimensional three-body system, Phys. Rev. A **100**, 012709 (2019).

[33] G. V. Skorniakov and K. A. Ter-Martirosian, Zh. Eksp. Teor. Fiz. **31**, 775 (1956) [Sov. Phys. JETP **4**, 648 (1957)].

[34] O. I. Kartavtsev, A. V. Malykh, and S. A. Sofianos, Bound states and scattering lengths of three two-component particles with zero-range interactions under one-dimensional confinement, J. Exp. Theor. Phys. **108**, 365 (2009).

[35] L. Du, P. Barral, M. Cantara, J. de Hond, Y.-K. Lu, and W. Ketterle, Atomic physics on a 50-nm scale: Realization of a bilayer system of dipolar atoms, Science **384**, 546 (2024).

[36] R. Zavin and N. Moiseyev, One-dimensional symmetric rectangular well: From bound to resonance via self-orthogonal virtual state, J. Phys. A: Math. Gen. **37**, 4619 (2004).

[37] L. M. Delves and J. L. Mohamed, *Computational Methods for Integral Equations* (Cambridge University Press, Cambridge, England, 1985).

[38] G. H. Golub and J. H. Welsch, Calculation of Gauss quadrature rules, Math. Comp. **23**, 221 (1969).